Mechanisms for O_2 dissociation over the BaO (100) surface

Nai-Xia Lu, Gang Fu, Xin Xu,[a),b)] and Hui-Lin Wan[a),c)]
State Key Laboratory for Physical Chemistry of Solid Surfaces and Center for Theoretical Chemistry, Institute of Physical Chemistry, Department of Chemistry, Xiamen University, Xiamen, 361005, People's Republic of China

(Received 20 August 2007; accepted 8 November 2007; published online 15 January 2008)

We have investigated the atomic and molecular oxygen adsorptions on the various sites of the BaO (100) surface with both cluster models and the periodic slab models. We found that the atomic oxygen prefers to adsorb on the surface O^{2-} to form the closed-shell peroxides with the binding energies of 83–88 kcal/mol. Such a high exothermicity provides a large driving force for the dissociation of molecular O_2 on the BaO surfaces. As molecular oxygen approaches the BaO surfaces, the triplet ground state O_2 molecule first binds electrostatically on top of the surface Ba^{2+} site. It further quenches to the singlet potential energy surface to form a covalently bonded O_3^{2-} species. We proposed a plausible pathway in which the O_3^{2-} species acts as the key precursor for further dissociation, leading eventually to the formation of surface peroxides O_2^{2-}. This mechanism is helpful for the understanding of a series of related catalytic processes such as the oxidative coupling of methane, the NO_x storage reduction, etc. © *2008 American Institute of Physics*. [DOI: 10.1063/1.2822178]

I. INTRODUCTION

The adsorption and dissociation of the molecular oxygen on the BaO surfaces play an important role in many types of heterogeneous catalysis. In the case of the oxidative coupling of methane (OCM), it was observed that the addition of barium to the rare-earth oxides or MgO catalysts could significantly enhance their catalytic performance.[1,2] Based on the results of the x-ray photoelectron spectroscopy and the *in situ* Raman spectroscopy, this enhancement was attributed to the increased amount of active oxygen species, O_2^{2-}, which came from the dissociative adsorption of O_2 on BaO, as a result of doping Ba to the OCM catalysts.[1,2]

Recently, with the introduction of the "lean-burn" engine technology, the effectiveness of the traditional three-way car emission catalysts is greatly degraded. The removal of harmful exhaust gases, in particular, the reduction of NO_x under such an oxygen rich condition, poses a great challenge to the development of novel catalysts. Among several catalysts developed so far, the NO_x storage-reduction (NSR) catalyst is particularly promising.[3] An important feature of the NSR catalyst is the presence of a highly efficient storage component, which can adsorb NO_x under the oxidizing condition and release NO_x under the reducing condition. The strongly basic metal-oxide BaO lends itself as an excellent candidate for such purpose. In the past several years, the storage of NO_x on BaO has been extensively studied.[4–12] With the *in situ* Raman spectroscopy, Hess and Lunsford found that the inclusion of 20% O_2 in the gas flow of NO_x at 400 °C led to an enhanced and direct nitrate formation without going through the nitrite formation step.[6] This was assumed to involve a direct NO_x reaction with the surface peroxides, whose formation was observed in the initial phase of the reaction.[6] On the other hand, the *in situ* Raman spectroscopy study of the decomposition of N_2O on the BaO surfaces showed that the addition of O_2 significantly inhibited the decomposition of N_2O.[13] The phenomena described above demonstrated the role that O_2 dissociation on the BaO surfaces played in the related heterogeneous catalytic processes.

As for the atomic oxygen adsorption on the alkaline-earth metal oxides, substantial amount of theoretical work has been reported.[14–18] These calculations revealed that atomic oxygen prefers to adsorb on the surface anion site rather than the surface cation site, forming a surface peroxide species, O_2^{2-}. The adsorption energies were found to increase down the group from MgO to BaO. This observation was related to the increased surface basicity going down from MgO to BaO due to the reduction of the Madelung potential along the expansion of the cation size.[19] As for the molecular adsorption of O_2 on the alkaline-earth metal-oxide surfaces, MgO is the most investigated system both experimentally[20–22] and theoretically.[23,24] These studies showed that O_2 was unbound or weakly bound on the nondefective surfaces. For the CaO surfaces, the desorption of singlet O_2 has been calculated and the results showed that the reoxidation of the surfaces by the desorbed O_2 could not occur.[25] The increased activity of the BaO surfaces infers that the molecular O_2 could adsorb and even dissociate on the surfaces, resulting in stable surface peroxides, which, in turn, serve as active oxygen species in several catalytic processes.[1,2,6]

Herein, we carried out a density functional theory study of molecular and atomic oxygen adsorptions on the BaO (100) surface, aiming to systematically address the possible dissociation mechanisms of O_2 on the BaO surfaces. To the

[a)]Authors to whom correspondence should be addressed.
[b)]Electronic mail: xinxu@xmu.edu.cn.
[c)]Electronic mail: hlwan@xmu.edu.cn.

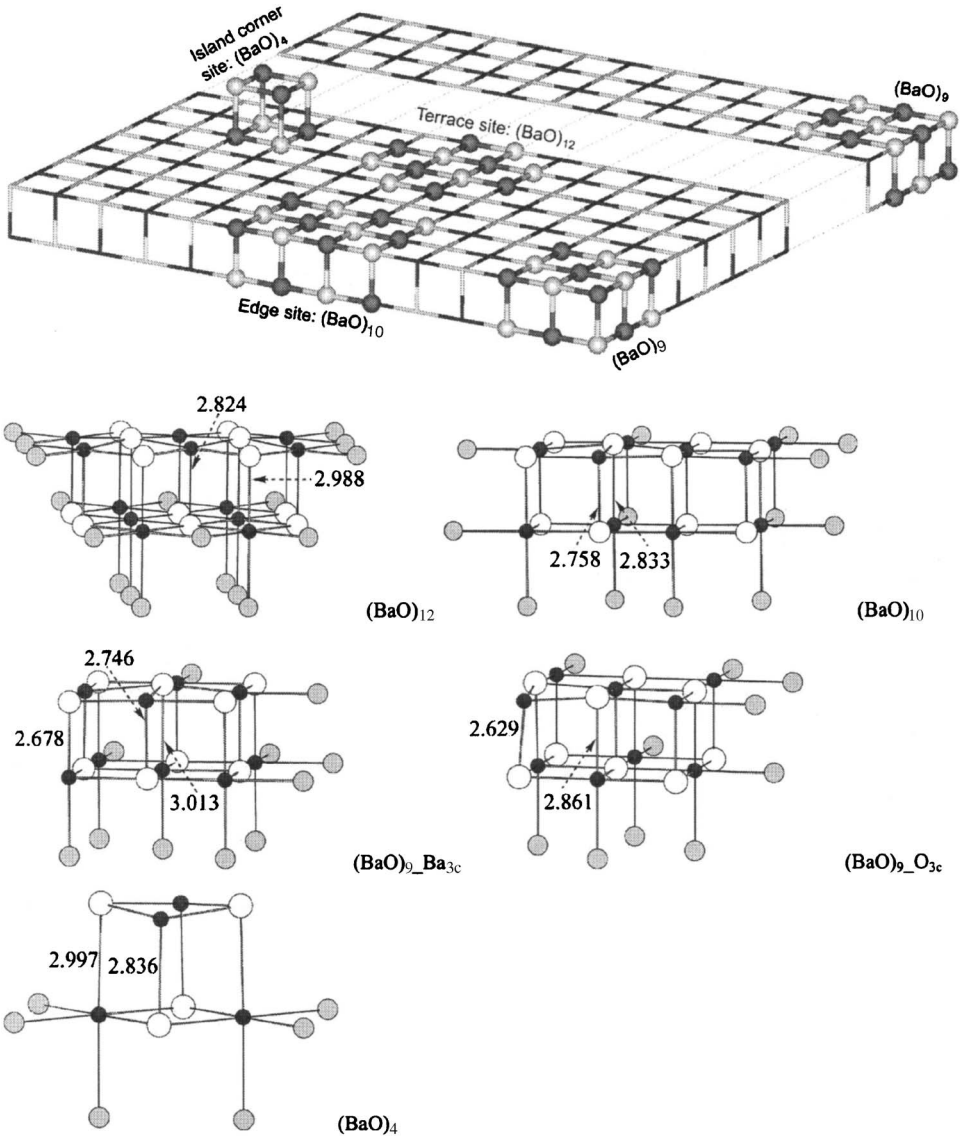

FIG. 1. Cluster models used in the present calculations. $(BaO)_{12}$, $(BaO)_{10}$, $(BaO)_9$, and $(BaO)_4$ are adopted to model the terrace, edge, corner, and island corner sites, respectively. Black balls stand for O and white balls for Ba. The gray spheres stand for the effective core potentials to represent Ba in close contact with the point charges (PCs). The PC array is depicted schematically. It is important to maintain the PC array symmetric so that there is no artificial dipole moment, created by the PC array, across the cluster. The island corner $(BaO)_4$ cluster should occupy the position similar to that of $(BaO)_{12}$. However, to aid our eyes, we have moved it aside.

best of our knowledge, such work has not been reported before.

II. COMPUTATIONAL DETAILS

Two strategies for describing the metal-oxide surfaces have been explored: the finite cluster model and the periodic slab method. Both methods have been widely used in the literature for the description of the adsorbate-metal-oxide interactions.[26–28] Here, we used cluster models to mimic the atomic and molecular oxygen adsorptions on the regular and various low-coordinated sites of the BaO (100) surface (see Fig. 1). These cluster models were constructed in fulfillment of some general requirements, namely, the neutrality principle, the stoichiometry principle, and the coordination principle.[29] The clusters used were $(BaO)_{12}$ for terrace (O_{5c} and Ba_{5c}), $(BaO)_{10}$ for edge (O_{4c} and Ba_{4c}), $(BaO)_9$ for corner (O_{3c} or Ba_{3c}), and $(BaO)_4$ for the island corner sites (see Fig. 1). All the selected model clusters were embedded in a large array of point charges (PCs). The charge magnitudes (± 1.73) of the PC array were determined self-consistently such that they are close to the averaged Mulliken charges of ions in the clusters.[18,29–31] As the clusters and the PC environment are both neutral (the neutrality principle) and the active sites for adsorption are all surrounded by real ions rather than PCs (the coordination principle), the effect of choosing the charges of the PC array on the active sites is significantly reduced. To circumvent the artificial polarization on the anion sites induced by the bordering positive PCs, total ion effective core potentials (ECPs), instead of positive PCs, were used at the cluster borders to represent the Ba cations.[32] The ions of the cluster which were not in direct contact with the PCs were all let free to relax in the geometry optimization, while the others in cluster were fixed to their bulk positions. The optimized structures of the clusters are displayed in Fig. 1, which show a negative rumpling of about 0.1–0.2 Å of the oxygen anions relative to the barium cations. This result is qualitatively in line with our findings from the periodic slab model calculations as discussed later.

The gradient-corrected Becke's three parameter hybrid exchange functional[33] in combination with the Lee-Yang-Parr[34] correlation functional (B3LYP) was used in all our cluster model calculations. The Ba atoms were treated with the relativistic ECPs and the corresponding valence ba-

sis sets were taken from the work of Hay and Wadt (LanL2dz).[35] The O atoms were described by using the 6 $-31+G^*$ basis set.[36] All density functional theory (DFT) calculations were performed by using the GAUSSIAN 03 suite of program.[36]

The interactions of the molecular O_2 with the BaO (100) surface were also calculated with the periodic slab model by using the commercial version of CASTEP.[37] The electronic energies and forces were calculated within the generalized gradient approximation (GGA) by using the Perdew-Burke-Ernzerhof (PBE) exchange-correlation functional.[38,39] Ultrasoft pseudopotentials[40] were adopted and the kinetic energy cutoff for the expansion of valence electronic wave function was set to be 300 eV. Within these approximations, bulk BaO has a lattice constant of 5.598 Å, 1.36% larger than the experimental value of 5.52.[41] The BaO (100) surface was represented with a $(\sqrt{2}\times\sqrt{2})$ supercell containing three atomic layers, and a 9 Å vacuum width was added in the surface normal to ensure no interactions between them. In the slab calculations, the bottom layer ions were kept frozen at the optimized bulk locations and the remaining ions were relaxed until the residual forces were smaller than 0.05 eV/Å. Surface distortions were divided into relaxation and rumpling. Relaxation refers to the interplane atomic movement, whereas rumpling measures the difference in anion and cation displacements. Here, the relaxation and rumpling were calculated to be −3.49% and −2.82%, respectively. These results are in good agreement with the previous findings (−3.6% and −3.0%) in the literature.[42] To make a direct comparison between the results from the slab model and the cluster model, some cluster model calculations on the terrace sites were carried out with the PBE functional.

III. RESULTS AND DISCUSSION

A. Atomic oxygen adsorption

We have examined the adsorption of atomic O on various sites of surface Ba^{2+} or O^{2-} in both singlet and triplet states. In agreement with the results from the previous study on the MgO surfaces by using the periodic slab methods,[23] we found that the atomic O is preferred to adsorb on the surface Ba^{2+} site in the triplet state and on the surface O^{2-} in the singlet state. As the global minima occur on the singlet potential energy surface and the triplets are metastable, we will only focus on the closed-shell singlet states, whose geometric configurations are presented in Fig. 2, and the corresponding adsorption energies E_{ad} are summarized in Table I. The E_{ad} were calculated by subtracting the sum of the energies of the isolated triplet ground state O atom and the corresponding cluster models from the energies of the optimized adsorbate-surface complexes. Such definition leads to a negative adsorption energy (or a positive binding energy) for an exothermic adsorption process.

As shown in Table I, charges on the active anion sites (O_s as labeled in Fig. 2) are −1.82 for O_{5c}, −1.72 for O_{4c}, −1.65 for O_{3c}, and −1.62 for island O_{3c}. These are in harmony with the embedding charges of ±1.73 of the PC array. Increasing the magnitudes of PCs to 2.0 will not change the charges on O_s strongly (<0.03 a.u.), as O_s in each model are surrounded by real ions, rather than PCs. Charges of ions on the cluster border are increased, leading to a larger difference in sites which should carry the same magnitude of charges. The calculated binding energies are in the range of 83–88 kcal/mol. Increasing the magnitude of the embedding charges only influences the calculated binding energies slightly (<0.2 kcal/mol). The distance between the adsorbed O and surface anion (O_s^{2-}) is about 1.5 Å, typically being within the bond length of the classical peroxide [1.49±0.02 (Ref. 43)], indicating the formation of peroxides on the surfaces. Significant charge transfer from the surface anion to the adsorbed O occurs. After adsorption, the magnitudes of negative charges on O_s are reduced to around −0.9 a.u. (see Table I). There is a nearly equal sharing of charges between O_s and O_{ad}, which also suggests the generation of the peroxide species. There is no net spin density, when the closed-shell peroxide species, O_2^{2-}, is formed.

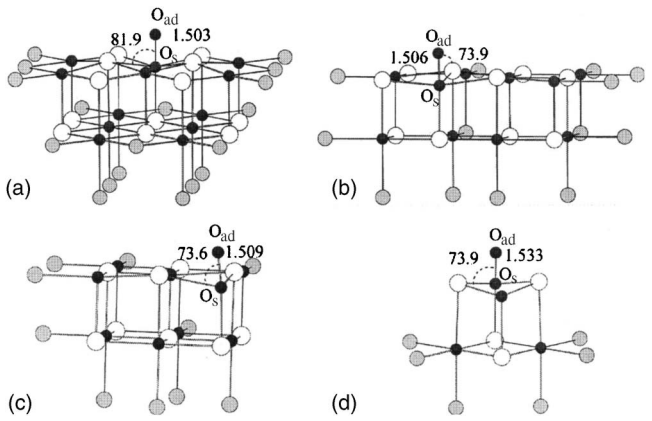

FIG. 2. The optimized geometries for singlet atomic O adsorption on the various sites of the BaO (100) surface. Selected distances and angles are in Å and degrees, respectively. Black balls stand for O and white balls for Ba. Point charges are not shown. The positive point charges at the borders, shown in gray balls, are represented by total ion effective core potentials.

We calculate the adsorption energy for the singlet O_{ad} on the terrace O_s^{2-} site as −82.8 kcal/mol. This number compares well to the previous calculation, where Karlsen *et al.* obtained −81.4 kcal/mol in their study of N_2O dissociation over a fully relaxed $(BaO)_5$ embedded cluster.[14] Very recently, Valentin *et al.* reported an embedded cluster model study on the formation of an oxygen vacancy and the simultaneous readsorption of an oxygen atom on the regular and the low-coordinated sites of the alkaline-earth oxide

TABLE I. Adsorption energies E_{ad} (in kcal/mol) and Mulliken charges Q for oxygen adsorption on the various sites of the BaO (100) surface.

Configuration	E_{ad}[a]	Q (O_{ad})[b]	Q (O_s)[c]
Terrace (O_{5c})	−82.8	−0.69	−0.90(−1.82)
Edge (O_{4c})	−82.6	−0.88	−0.95(−1.72)
Corner (O_{3c})	−84.3	−0.85	−0.94(−1.65)
Island Corner (O_{3c})	−88.4	−0.89	−0.90(−1.62)

[a]Adsorption energies are referred to the ground state oxygen atom and the corresponding free surface models.
[b]Mulliken charges for the adsorbed oxygen atoms.
[c]Mulliken charges for the surface oxygen ions (O_s as marked in Fig. 2) after adsorptions. The corresponding data before adsorption are listed in parentheses.

surfaces.[15] A similar adsorption energy (−82.1 kcal/mol) was reported on the terrace site. Valentin *et al.*[15] found that, on MgO(100), the peroxo complex was tilted by about 30° with respect to the surface normal. This was attributed to the electrostatic effects. On the (100) surfaces of CaO, SrO, and BaO, however, they found that the peroxo complex was oriented normal to the surface because the lattices were expanded and the electrostatic effects were reduced.[15] It is very plausible that this tilted angle decreases gradually along this series from MgO to BaO. Indeed, we find that the electrostatic effect can still play a role even for the terrace site of BaO (100), leading to a tilted geometry with a calculated $O_{ad}-O_s-Ba$ angle of 81.9°. While Valentin *et al.* found that the upright geometries remained when going from the terrace to the edge and corner site, we find a gradual bending toward a surface $O^{2-}-Ba^{2+}$ bond, with $O_{ad}-O_s-Ba$ angle being 74° (see Fig. 2). With respect to the surface normal, the tilted angles are calculated to be 4.1°, 6.2°, and 11.3° for the terrace, edge, and corner sites, respectively. If we increase the magnitude of embedding charges to ±2.0, the $O_{ad}-O_s-Ba$ angle on the terrace site is calculated to be 80.9°, bending toward the surface Ba^{2+} by another 1°. In terms of O-atom adsorption energy, however, the difference is only 0.2 kcal/mol, suggesting that the electrostatic effects in this case may have a larger influence on the geometry than on the adsorption energy.

It would be very interesting to examine how the lattice relaxation will affect the adsorption energy. With the surface lattice being fixed to the ideal position in the bulk, the adsorption energy for the singlet O_{ad} on the terrace O_s^{2-} site is calculated to be −68.8 kcal/mol. Allowing only the surface anion site to relax in the optimization leads to an increased adsorption energy to −80.1 kcal/mol. Further allowing all the lattice ions of the cluster which are not in direct contact with the PCs to relax increases the adsorption energy to −82.8 kcal/mol. Hence, the relaxation of the lattice ion which is directly under the O_{ad} is the most significant. Another interesting finding is that surface relaxation affects most the adsorption energy of the terrace site. Thus, relaxation of the terrace cluster gives an energy difference of 14.0 kcal/mol as compared to the fixed terrace model. Such a difference is decreased to 9.1 for the edge models, 4.5 for the corner model, and only 0.3 kcal/mol for the island corner models. Hence, surface relaxation is seen to diminish the difference between various sites for the atomic O adsorption.

The calculated stretching frequencies for the surface peroxide are between 822 and 907 cm^{-1} for various sites. Valentin *et al.* have computed the vibrational frequencies for the peroxo groups and obtained values of 898–953 cm^{-1} at various oxides.[15] They suggested that peroxo groups formed at various sites of the alkaline-earth oxides have very similar vibrational signatures and concluded that this vibration is not diagnostic of the oxide nor of the site where the complex is formed.[15] In general, peroxides are expected to exhibit vibrational frequencies in the 800–900 cm^{-1} region. We noticed that Hess and Lunsford suggested that a band at 930 cm^{-1} was due to peroxo groups formed on the surface of BaO,[6] and Au *et al.* located a peroxide peak of 927 cm^{-1} on the BaO/Gd_2O_3 catalysts.[2] Hence, our computed values are consistent with some experimental values reported in the literature.[2,15]

So far, we have displayed that the formation of peroxide species via singlet oxygen attached to surface anion is favored thermodynamically. Although previous studies have indicated that surface peroxide species could be generated through molecular O_2 adsorption on the *F* center of metal oxides,[44] the concentration of the *F* center is too low to play an important role in a real catalytic process, normally carried out at relatively high temperature.[15,45] We are curious whether the peroxide species could be generated by an O_2 direct dissociation on the BaO surface without using an *F* center. In the next content, we will report the details of such process as $O_2+2\ O^{2-}\rightarrow 2\ O_2^{2-}$.

B. The molecular oxygen adsorption

It is well-known that the ground state for the molecular oxygen is an open-shell triplet ($^3\Sigma^-_g$), and there are two low-lying singlet states, $^1\Delta_g$ and $^1\Sigma^+_g$, with the energy gaps of 22.6 and 37.7 kcal/mol, respectively, relative to the ground state.[46] If the triplet ground state O_2 dissociates on the closed-shell BaO surface, leading to the peroxide species in the singlet state, there should exist a spin-state flipping from the triplet potential energy surface to the singlet potential energy surface. Recently, laser Raman spectroscopy study on the La_2O_3 catalysts demonstrated that the laser not only served as an excitation source for Raman scattering but also induced the formation of peroxides on the surfaces.[47] We present here our calculation results on triplet and singlet O_2 adsorptions on various sites of the BaO surfaces. Figure 3 depicts the predicted adsorption geometries and Table II summarizes the corresponding adsorption energies with respect to the ground state energy of $^3O_2$.

Taking O_2 adsorption on the terrace site as an instructive example, it is clearly seen that the triplet O_2 is brought to the surface Ba ions with a bent configuration. Due to the charge transfer from the surface to the antibonding π^* orbital of O_2, the O_2 molecule is negatively charged by 0.40 and the bond length of the adsorbed O_2 is elongated to 1.29 Å, which can be compared with the calculated bond length of free O_2 of 1.21 Å. The distance of the O_{ad} from the nearest surface Ba^{2+} is 3.08–3.21 Å, being longer than the Ba–O distance in the bulk lattice [2.76 Å (Ref. 41)]. The adsorption energy on the terrace Ba^{2+} site (Ba_{5c}) is −10.8 kcal/mol. The binding energies increase slightly to 14.1 and 13.8 kcal/mol on the edge and corner sites, respectively. It significantly increases to 35.5 kcal/mol for the island corner site. We see that charge transfers to the molecular O_2 are slightly increased to 0.47 and 0.48 for the corner and edge sites, respectively. It is more than doubled for the island corner site.

The situation of the singlet O_2 adsorption on the same surface is quite different. Instead of binding to the surface Ba^{2+} sites, singlet O_2 binds to the surface anion sites. The local minimum for the terrace site is found where O_2 is tiltedly adsorbed on the surface O_{5c} site exothermically by 15.0 kcal/mol. Significant charge transfer from the surface anion to the adsorbed $^1O_2$ leads to a negatively charged O_2

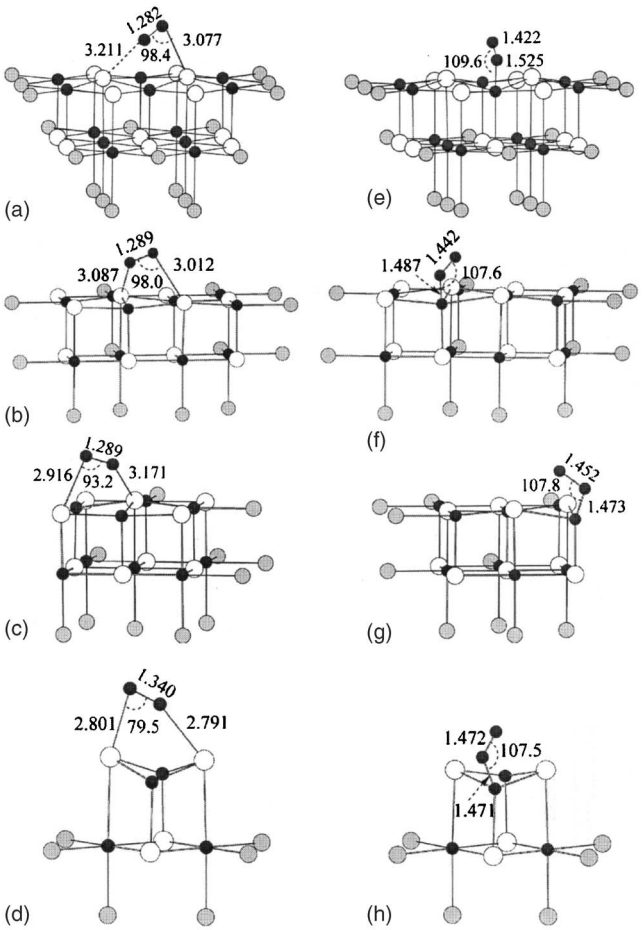

FIG. 3. Optimized geometries for molecular oxygen adsorption on the terrace, edge, and island sites, respectively. (a)–(d) are for triplet states and (e)–(h) are for singlet states. Selected distances are given in Å and angles in degrees. Black balls stand for O and white balls for Ba. Point charges are not shown. The positive point charges at the borders, shown in gray balls, are represented by total ion effective core potentials.

by 0.88 and the bond length of O_2 increased to 1.42 Å. Additionally, the distance between the surface anion and adsorbed O is only 1.53 Å, which indicates that the O_2 π bond strength is reduced and, simultaneously, a new σ bond is created to form a new unit of O_3^{2-}. This O_3^{2-} species has been proposed before on the $Th-La-O_x/BaCO_3$-based OCM catalysts,[48] which we propose here may act as an precursor for its further dissociation. The binding energies increase steadily from the terrace site to the edge, corner, and island corner sites. For all sites, there exists a significant amount of charge transfer (0.81–0.91) and the O_3^{2-} unit can be envisioned. The stretching frequencies calculated for O_3^{2-}

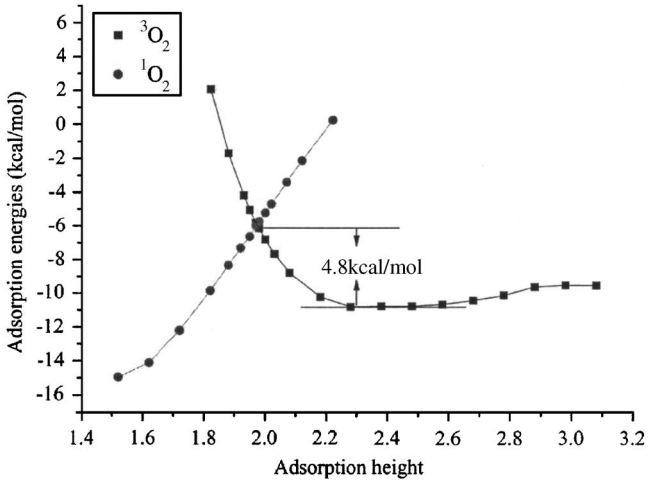

FIG. 4. Potential energy curves for the adsorption of molecular oxygen on the $(BaO)_{12}$ cluster in the singlet and triplet states. The energies are referenced to the ground state O_2 plus the corresponding free surface models.

on the terrace, edge, corner, and island corner sites are 924, 916, 913 and 889 cm^{-1}, respectively. We recall that a previous Raman experiment has observed a peak at around 930–960 cm^{-1} on the $Th-La-O_x/BaCO_3$-based OCM catalysts, which has been tentatively ascribed to the O_3^{2-} species.[48]

We notice that the lattice relaxation increases the stability of the $^1O_2$ adsorption more significantly than that of the $^3O_2$ adsorption. Hence, the $^1O_2$ adsorptions on the terrace and edge sites are stabilized by about 13.0 and 9 kcal/mol on the corner site and 6 kcal/mol on the island corner site upon relaxation, while the relaxation stabilization for the $^3O_2$ adsorption is only around 3.0 kcal/mol on the terrace and edge, making the singlet O_3^{2-} species lower lying on the potential energy surfaces than the corresponding adsorbed state of triplet O_2 (see Table II).

Now, our calculations locate two adsorption configurations when molecular O_2 approaches the BaO surfaces: one (far away, ~3.0 Å, from the surface) is in the triplet state, where $^3O_2$ binds to the surface Ba^{2+} mainly electrostatically, and the other (in close proximity, ~1.5 Å, to the surface) is in the closed-shell singlet state, where $^1O_2$ binds to the surface O^{2-} covalently. With the heavy-atom effect of barium, it is conceivable that the adsorbed triplet O_2 crosses over the singlet state potential energy surface to form the more stable O_3^{2-} intermediate, such that the dissociation channel from O_2 to O_2^{2-} is open.

Figure 4 displays the detailed dissociation energy curves

TABLE II. O_2 adsorption in triplet and closed-shell singlet: Binding energies (E_{ad}; kcal/mol), as well as charges and spin densities on the adsorbed O_2 as obtained from Mulliken population analysis.

$^3O_2$				$^1O_2$		
Adsorption site	Charge	Spin density	E_{ad}	Adsorption site	Charge	E_{ad}
Island corner	−0.94	0.98	−35.48	Island corner	−0.91	−37.90
Corner	−0.47	1.42	−13.75	Corner	−0.81	−30.21
Edge	−0.48	1.42	−14.07	Edge	−0.85	−20.99
Terrace	−0.40	1.48	−10.76	Terrace	−0.88	−14.95

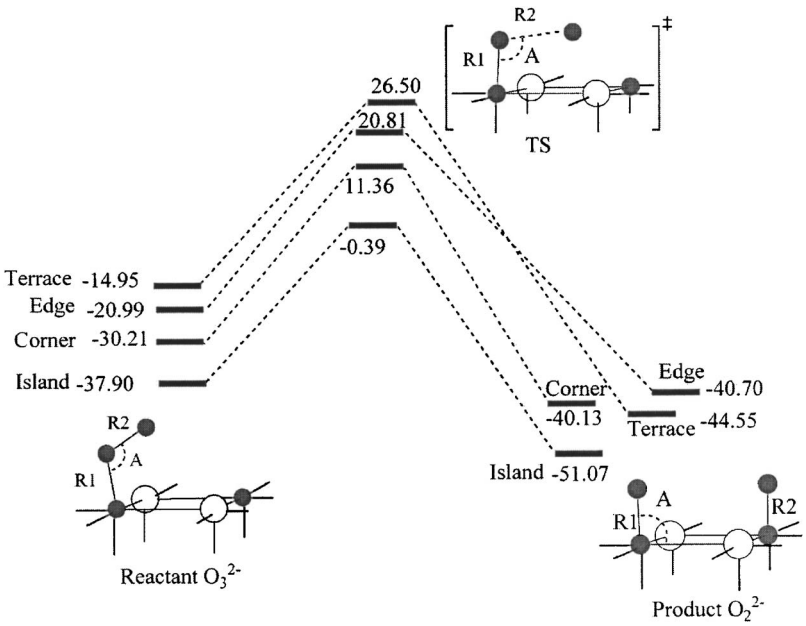

FIG. 5. Dissociation of O_3^{2-} on the terrace, edge, corner, and island corner sites. Black balls stand for O and white balls for Ba. Point charges are not shown. The energies are referenced to the ground state O_2 plus the corresponding free surface models.

on a $(BaO)_{12}$ terrace model, where we monitor the adsorption energy changes, both in triplet and closed-shell singlet, with the adsorption height of O_2 from the nearest surface anion. We start with an initial configuration where the molecular O_2 is declined toward the surface. While O_2 is far from the surface (>1.9 Å), the triplet state is lower in energy than the singlet state. As O_2 moves toward the surface in the triplet state, this motion finds an upward valley on the potential surface. In contrast, as $^1O_2$ moves down the surface, the energy curve drops precipitously by 15.0 kcal/mol. The crossing point is $R(O-O_s^{2-})=1.97$ Å (Fig. 4). In this way, we find that the conversion from the spin triplet state to the spin singlet state may eventually occur by overcoming a spin barrier of 4.8 kcal/mol. We recall that the excitation energy required from the ground state O_2 to two low-lying singlet states, $^1\Delta_g$ and $^1\Sigma^+_g$, are 22.6 and 37.7 kcal/mol, respectively.[46] Therefore, it is likely that the spin-orbit interaction plays a role here, which facilitates the spin crossover from triplet to singlet potential energy surface. As for the cases of O_2 adsorptions on the edge and corner sites of the BaO surfaces, a similar picture can be envisioned.

Previously, the problem of how triplet O_2 dissociates on the singlet potential energy surface has been studied before on other surfaces [i.e., O_2/Al(111),[49] O_2/carbon nanotube,[50] and O_2/Si(100) (Ref. 51)] by using DFT methods. However, it is important to notice that DFT methods may have difficulties in describing the open-shell singlet.[52] While here, we only focus on the closed-shell singlet, which is the main character of system at short O_s-O_{ad} distance, open-shell singlet may also play a role at the point of spin crossover. Nevertheless, it is conceivable that the multireference contribution will further decrease the spin crossover barrier.

C. The dissociation of O_3^{2-} on the BaO surface

In this section, we proceed to the dissociation of O_3^{2-} on the BaO surfaces, leading to the surface peroxo species. The optimized geometries and the corresponding potential energy curves are shown in Fig. 5, and the geometric parameters corresponding to the reactants (O_3^{2-}), the transition states (TS), and the products (O_2^{2-}) are summarized in Table III. All species are found in closed-shell singlet.

As is clearly seen in Fig. 5 and Table III, the general feature of the dissociation is that the adsorbed $^1O_2$ molecule (i.e., O_3^{2-}) expands its bond length toward the adjacent surface oxygen ion, and through a late transition state [$R_2(O-O)=2.07-2.46$ Å], eventually two surface peroxo species are generated. In these processes, an intrinsic barrier of ~41 kcal/mol is identified for either the terrace or the edge sites. The corner sites are more reactive, with a reduced barrier of ~38 kcal/mol. With respect to the ground state $^3O_2$, the high stability of O_3^{2-} on the island corner site actually brings the transition state down to −0.4 kcal/mol lower than the entrance level, lending this process with no apparent barrier.

Regardless of the active surface sites, the optimized O–O distance in the products is ~1.50 Å, characteristic of a classical peroxide. The calculated frequency for the terrace

TABLE III. Geometry parameters for singlet O_2 dissociation on the different sites.

Configuration	Bond length (Å) and angle (deg)	Reactant O_3^{2-}	TS	Product O_2^{2-}
Terrace	*R*1	1.525	1.466	1.504
	*R*2	1.423	2.195	1.504
	A	109.6	100.7	81.7
Edge	*R*1	1.487	1.466	1.507
	*R*2	1.442	2.127	1.501
	A	107.6	101.4	85.6
Corner	*R*1	1.473	1.459	1.508
	*R*2	1.452	2.067	1.501
	A	107.8	101.9	73.3
Island corner	*R*1	1.471	1.433	1.528
	*R*2	1.472	2.464	1.528
	A	107.5	103.8	88.0

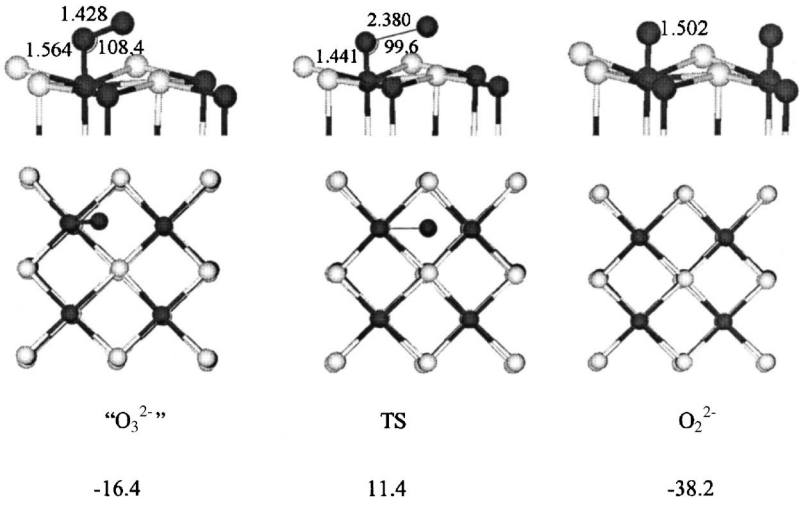

FIG. 6. Optimized geometries and reaction energies for the O_3^{2-} dissociation process with the slab model calculations. The energies are referenced to the ground state O_2 plus the corresponding free surface models. Black balls stand for O and white balls for Ba.

peroxide is around 904 cm^{-1}, in good agreement with the value of 927 cm^{-1} observed in the experiment.[2] There exists subtle difference in the bonding angles. While O_{ad} sits almost upright on the O_{4c} site, it bends slightly outward and inward on the O_{5c} and O_{3c} sites, respectively.

The lattice relaxation is found to be important for the O_3^{2-} dissociation. Thus, as discussed above, the terrace and edge O_3^{2-} are stabilized by ~13.0 kcal/mol when the lattice relaxation is taken into account. This correlates well with the observation that the relaxed O anions are moved inward by 0.1–0.2 Å, resulting in a larger Madelung stabilization. This effect is less significant for the transition state, as turning on the lattice relaxation stabilizes the transition states by 8.4 and 5.6 kcal/mol for the terrace and edge sites, respectively. Hence, the intrinsic barriers related to the O_3^{2-} species are reduced by 5–10 kcal/mol from terrace to corner sites upon relaxation. The relaxation effect is even more profound for the O_2^{2-} product. After relaxation, we find that the overall reaction: $^3O_2+2\ O^{2-} \rightarrow 2\ O_2^{2-}$ is exothermic by 40.1, 40.7, and 44.6 kcal/mol for the corner, edge, and terrace sites, respectively. These compare well with the experimental value of 36.1 kcal/mol.[53] Without taking into account the lattice relaxation, however, the corresponding exothermicities are too small by 18.6–26.1 kcal/mol, which are way off from the experimental data.

The lateral interaction on the O-atom adsorbed surfaces can be estimated using the cluster model results. We calculated ΔH_1 for $^3O_2 \rightarrow 2\ ^3O$ to be 120.0 kcal/mol. From Table I, we know that ΔH_2 for $^3O+O_{5c}^{2-} \rightarrow (O_{5c}-O)^{2-}$ is −82.8 kcal/mol. Combining these two results, we have $\Delta H_3=\Delta H_1+2\ \Delta H_2=-45.6$ kcal/mol for the reaction of $^3O_2+2\ O_{5c}^{2-} \rightarrow 2\ (O_{5c}-O)^{2-}$. On the other hand, from Fig. 5, we know that the exothermicities for triplet O_2 to dissociate on the terrace sites is −44.6 kcal/mol. Hence, the lateral interaction between a pair of adsorbed O atoms is around 1.0 kcal/mol.

We also check the B3LYP cluster model calculations on the terrace against the periodic slab calculations. As the slab calculations are performed by using the PBE functional, cluster model calculations are also carried out with PBE. Our optimized geometries for the terrace site by using the periodic slab method are shown in Fig. 6, which compare well with the cluster model results shown in Fig. 5 and Table III. The slab model predicts that the reactant O_3^{2-} lies at −16.4 kcal/mol with respect to the free surface and the ground state O_2. This number is in good agreement with the results based on the cluster model calculations (−15.0 for B3LYP and −18.5 for PBE). The slab model shows that the product O_2^{2-} lies at −38.2 kcal/mol. This number is also in good accordance with the cluster model results (−44.6 for B3LYP and −42.0 for PBE). The slab model calculates the intrinsic barrier to be 27.8 kcal/mol with respect to the reactant O_3^{2-}. This number is, however, low as compared to the B3LYP value (41.5) based on the cluster model. The PBE functional contributes a significant difference to the barrier height. In fact, we have encountered difficulty in locating the transition state within the cluster model by using PBE. Adopting the geometry optimized by the B3LYP functional, the transition state predicted by PBE is 7.1 kcal/mol lower than the B3LYP value. It is known that GGA functionals tend to underestimate the barrier.[54–56] All in all, we conclude that our B3LYP cluster model results are reliable, especially when the trends between the different surface sites are concerned.

D. Discussion

As is well-known, the surface chemistry of the cubic alkaline-earth oxides (MgO, CaO, SrO, and BaO) is dominated by the basicity of surface anion O^{2-}.[19] This basicity increases down the alkaline-earth family as the crystal lattice expands and metal ions become more electropositive.[19] The direct consequence is that the valence state of surface O^{2-} in MgO lies in lower energy (more stable) than that in BaO.[19,45] In this way, it is not surprising to find that O_2 could not be dissociatively adsorbed on the vacancy-free MgO surface and peroxide ions are hardly detected,[20–22] whereas on the BaO surface, in the presence of oxygen under the working conditions of the NO_x-storage catalyst, a large amount of peroxides has been indeed observed, which, in turn, accelerates the NO_x storage.[6] The ability of BaO to easily form peroxo species from molecular O_2 could, thus, be a key point in understanding the specific efficiency of BaO for NO_x storage. Our cluster model calculations show that the apparent

activation barrier on the terrace site is about 27 kcal/mol with respect to $^3O_2$. Thus, it is conceivable that surface O_2^{2-} species can be formed directly over the BaO surfaces under typical OCM operating conditions (650–850 °C).[57]

It is interesting to notice that our calculated apparent activation energy on the terrace site is close to that of N_2O dissociation on the BaO surfaces, 33 kcal/mol, estimated in a recent experiment work of Xie and Lunsford.[13] The mechanism of the N_2O decomposition reaction on the earth-alkaline oxide was suggested as follows:

$$N_2O + O^{2-} \rightarrow N_2 + O_2^{2-}, \quad (1)$$

$$O_2^{2-} + O_2^{2-} \rightarrow O_2 + 2O^{2-}. \quad (2)$$

Step (1) is the N_2O dissociatively adsorbed on the surface anion to form surface peroxide species. Step (2) is the generation of the surface anions by desorption of molecular oxygen. The experimental work by Xie and Lunsford has shown a strong inhibiting effect when adding O_2 to the reaction system. The similar barrier predicted in this calculation for the reverse reaction of step (2) suggests that the O_2 dissociation competes with the N_2O dissociation. Our results also suggest that the oxygen recombination from O_2^{2-}, as shown in step (2) is not a working mechanism on the BaO surfaces, as a barrier as high as 71 kcal/mol will be encountered, as shown in Fig. 5. This is in agreement with the conclusion of Karlsen *et al.* on the N_2O dissociation.[14]

IV. CONCLUSIONS

We have investigated the atomic and molecular oxygen adsorptions on various sites of the BaO surfaces. Our main conclusions can be summarized as follows:

(1) We find that the global minima for atomic O adsorption are to form the closed-shell peroxides with the binding energies of 83–88 kcal/mol for various sites with respect to the ground state ^3O atom. Lattice relaxation is found to increase the binding energy of the terrace site most, diminishing, to a large extent, the site dependence. We assume that the formation of stable peroxides provides a large driving force for the dissociation of molecular O_2 on the BaO surfaces.

(2) We find that both triplet and singlet molecular oxygen can adsorb on the strongly basic BaO surfaces. As molecular oxygen approaches the BaO surfaces, the triplet ground state O_2 molecule first binds electrostatically on top of the surface Ba^{2+} [$R(O_{ad}–Ba^{2+}) \approx 3.0$ Å]. It further quenches to the singlet potential energy surface to form a covalently bounded O_3^{2-} species. We calculate the spin transition barrier on the terrace site to be around 4.8 kcal/mol.

(3) We suggest the O_3^{2-} species be the key precursor for further dissociation, leading to the formation of surface peroxides O_2^{2-}. With respect to the triplet ground state of molecular oxygen, the apparent dissociation barriers are calculated to be 26.5, 20.8, and 11.4 kcal/mol, respectively, for the terrace, edge, and corner sites. With respect to the ground state $^3O_2$, the high stability of O_3^{2-} on the island corner site actually brings the transition state down to −0.4 kcal/mol lower than the entrance level, lending this process with no apparent barrier.

(4) The lattice relaxation is found to play a variable role for the reactants, transition states, and the products for the O_3^{2-} dissociation process over different sites on the BaO (100) surface. For example, while the terrace and edge O_3^{2-} are stabilized by ~13.0 kcal/mol, the transition states are stabilized by 8.4 and 5.6 kcal/mol for the terrace and edge sites, respectively, upon lattice relaxation. The relaxation effect is even more profound for the O_2^{2-} product, giving 26.1 and 19.0 kcal/mol stabilizations for the terrace and edge sites.

(5) Our theoretical results support the experimental observation for the existence of surface peroxides in the related oxidative coupling of methane and the NO_x-storage reduction in the presence of O_2/BaO. Moreover, our results suggest an inhibiting role played by O_2 in the decomposition of N_2O on the BaO surfaces, in agreement with the experimental observation.

ACKNOWLEDGMENTS

This work was supported by National Natural Science Foundation of China (Nos. 20525311, 20533030, and 20433030) and the Ministry of Science and Technology (Nos. 2007CB815206 and 2005CB221408).

[1] J. H. Lunsford, X.-M. Yang, K. Haller, and J. Laane, J. Phys. Chem. **97**, 13810 (1993).
[2] C. T. Au, K. D. Chen, and C. F. Ng, Appl. Catal., A **170**, 81 (1998).
[3] N. Takahashi, H. Shinjoh, T. Iijima, T. Suzuki, K. Yamazaki, K. Yokota, H. Suzuki, N. Miyoshi, S. Matsumoto, T. Tanizawa, T. Tanaka, S. Tateishi, and K. Kasahara, Catal. Today **27**, 63 (1996).
[4] E. Fridell, H. Persson, B. Westerberg, L. Olsson, and M. Skoglundh, Catal. Lett. **66**, 71 (2000).
[5] H. Mahzoul, J. F. Brilhac, and P. Gilot, Appl. Catal., B **20**, 47 (1999).
[6] C. Hess and J. H. Lunsford, J. Phys. Chem. B **106**, 6358 (2002).
[7] L. Olsson, H. Persson, E. Fridell, M. Skoglundh, and B. Andersson, J. Phys. Chem. B **105**, 6895 (2001).
[8] P. J. Schmitz and R. J. Baird, J. Phys. Chem. B **106**, 4172 (2002).
[9] C. Sedlmair, K. Seshan, A. Jentys, and J. A. Lercher, J. Catal. **214**, 308 (2003).
[10] I. Nova, L. Castoldi, L. Lietti, E. Tronconi, and P. Forzatti, Catal. Today **75**, 431 (2002).
[11] W. S. Epling, L. E. Campbell, A. Yezerets, N. W. Currier, and J. E. Parks II, Catal. Rev. - Sci. Eng. **46**, 163 (2004).
[12] Z. M. Liu and S. I. Woo, Catal. Rev. - Sci. Eng. **48**, 43 (2006).
[13] S. Xie and J. H. Lunsford, Appl. Catal., A **188**, 137 (1999).
[14] E. J. Karlsen, M. A. Nygren, and L. G. M. Pettersson, J. Phys. Chem. A **106**, 7868 (2002).
[15] C. D. Valentin, R. Ferullo, R. Binda, and G. Pacchioni, Surf. Sci. **600**, 1147 (2006).
[16] W. S. Abdel Halim and A. S. Shalabi, Solid State Commun. **124**, 67 (2002).
[17] M. A. Nygren and L. G. M. Pettersson, Chem. Phys. Lett. **230**, 456 (1994).
[18] X. Lu, X. Xu, N. Q. Wang, and Q. E. Zhang, J. Phys. Chem. B **103**, 3373 (1999).
[19] G. Pacchioni, J. M. Ricart, and F. Illas, J. Am. Chem. Soc. **116**, 10152 (1994).
[20] Y. Yanagisawa, R. Mitsuhashi, K. Matsumura, and S. Yamabe, Surf. Sci. **242**, 513 (1991).
[21] M. Che and A. J. Tench, Adv. Catal. **32**, 1 (1983).
[22] J. H. Lunsford and J. P. Jayne, J. Chem. Phys. **44**, 1487 (1966).
[23] L. N. Kantorovich and M. J. Gillan, Surf. Sci. **374**, 373 (1997).
[24] G. Pacchioni, A. M. Ferrari, and E. Giamello, Chem. Phys. Lett. **255**, 58

(1996).
[25] S. Anders and P. Itai, J. Chem. Phys. **103**, 7626 (1995).
[26] H. Grönbeck, Top. Catal. **28**, 59 (2004).
[27] J. Sauer, P. Ugliengo, E. Garrone, and V. R. Saunders, Chem. Rev. (Washington, D.C.) **94**, 2095 (1994).
[28] E. A. Colbourn, Surf. Sci. Rep. **15**, 281 (1992).
[29] X. Xu, H. Nakatsuji, X. Lu, M. Ehara, Y. Cai, N. Q. Wang, and Q. E. Zhang, Theor. Chem. Acc. **102**, 170 (1999).
[30] X. Xu, H. Nakatsuji, M. Ehara, X. Lu, N. Q. Wang, and Q. E. Zhang, Sci. China, Ser. B: Chem. **41**, 113 (1998).
[31] X. Xu, H. Lu, N. Q. Wang, and Q. E. Zhang, Chem. Phys. Lett. **235**, 546 (1995).
[32] N. W. Winter, R. M. Pitzer, and D. K. Temple, J. Chem. Phys. **86**, 3549 (1987).
[33] A. D. Becke, J. Chem. Phys. **98**, 5648 (1993).
[34] C. Lee, W. Yang, and R. G. Parr, Phys. Rev. B **37**, 785 (1988).
[35] P. J. Hay and W. R. Wadt, J. Chem. Phys. **82**, 299 (1985).
[36] M. J. Frisch, G. W. Trucks, H. B. Schlegel *et al.*, GAUSSIAN 03, revision B.3, Gaussian, Inc., Pittsburgh, PA, 2003.
[37] M. C. Payne, D. C. Allan, T. A. Arias, and J. D. Johannopoulus, Rev. Mod. Phys. **64**, 1045 (1992).
[38] J. P. Perdew and Y. Wang, Phys. Rev. B **45**, 13244 (1992).
[39] J. P. Perdew, J. A. Chevary, S. H. Vosko, K. A. Jackson, M. R. Pederson, D. J. Singh, and C. Fiolhais, Phys. Rev. B **46**, 6671 (1992).
[40] D. Vanderbildt, Phys. Rev. B **41**, 7892 (1990).
[41] Z. P. Chang and G. R. Barsch, J. Geophys. Res. **74**, 3291 (1969).
[42] P. Broqvist, I. Panas, and H. Grönbeck, J. Phys. Chem. B **109**, 15410 (2005).
[43] M. S. Palmer and M. Neurock, J. Phys. Chem. B **106**, 6543 (2002).
[44] M. S. Palmer, M. Neurock, and M. M. Olken, J. Am. Chem. Soc. **124**, 8452 (2002).
[45] G. Pacchioni, Solid State Sci. **2**, 161 (2000).
[46] J. T. Vanderslice, E. A. Mason, and W. G. Maisch, J. Chem. Phys. **32**, 515 (1960); G. Herzberg, *Molecular Spectra and Molecular Structure* (Van Nostrand, Princeton, NJ, 1966), p. 560.
[47] W. Z. Weng, H. L. Wan, J. M. Li, and Z. X. Cao, Angew. Chem., Int. Ed. **43**, 975 (2004).
[48] H. B. Zhang, G. D. Lin, H. L. Wan, W. Z. Weng, J. X. Cai, Y. F. Shen, and K. R. Tsai, Catal. Lett. **73**, 141 (2001).
[49] J. Behler, B. Delley, S. Lorenz, K. Reuter, and M. Scheffler, Phys. Rev. Lett. **94**, 036104 (2005).
[50] S. P. Chan, G. Chen, X. G. Gong, and Z. F. Liu, Phys. Rev. Lett. **90**, 086403 (2003).
[51] X. L. Fan, Y. F. Zhang, W. M. Lau, and Z. F. Liu, Phys. Rev. Lett. **94**, 016101 (2005).
[52] D. Cremer, Mol. Phys. **99**, 1899 (2001).
[53] M. Königstein and C. R. A. Catlow, J. Solid State Chem. **140**, 103 (1998).
[54] A. Ruzsinszky, J. P. Perdew, and G. I. Csonka, J. Phys. Chem. A **109**, 11006 (2005).
[55] Y. Kanai, X. Wang, A. Selloni, and R. Car, J. Chem. Phys. **125**, 234104 (2006).
[56] C. Tuma and J. Sauer, Chem. Phys. Lett. **387**, 388 (2004).
[57] V. R. Choudhary, V. H. Rane, and S. T. Chaudhari, Appl. Catal., A **158**, 121 (1997).